Available online at www.sciencedirect.com
ScienceDirect
Remote Sensing of Environment 112 (2008) 337–349
Remote Sensing of Environment
www.elsevier.com/locate/rse

Effect of remote sensing spatial resolution on interpreting tower-based flux observations

Fuqin Li [a,*], William P. Kustas [a], Martha C. Anderson [a], John H. Prueger [b], Russell L. Scott [c]

[a] USDA-ARS Hydrology and Remote Sensing Lab, Bldg. 007, BARC-West, Beltsville, MD 20705, United States
[b] USDA-ARS National Soil Tilth Lab, 2150 Pammel Dr., Ames, IA 50011, United States
[c] USDA-ARS Southwest Watershed Research Center, Tucson, AZ 85719, United States

Received 21 July 2006; received in revised form 14 November 2006; accepted 18 November 2006

Abstract

Validation comparisons between satellite-based surface energy balance models and tower-based flux measurements over heterogeneous landscapes can be strongly influenced by the spatial resolution of the remote sensing inputs. In this paper, a two-source energy balance model developed to use thermal and visible /near-infrared remotely sensed data is applied to Landsat imagery collected during the 2004 Soil Moisture Experiment (SMEX04) conducted in southern Arizona. Using a two dimensional flux-footprint algorithm, modeled surface fluxes are compared to tower measurements at three locations in the SMEX04 study area: two upland sites, and one riparian site. The effect of pixel resolution on evaluating the performance of the land surface model and interpreting spatial variations of land surface fluxes over these heterogeneous areas is evaluated. Three Landsat scenes were examined, one representing the dry season and the other two representing the relatively wet monsoon season. The model was run at three resolution scales: namely the Landsat visible/near-infrared band resolution (30 m), the Landsat 5 thermal band resolution (120 m), and 960 m, which is nominally the MODIS thermal resolution at near-nadir. Comparisons between modeled and measured fluxes at the three tower sites showed good agreement at the 30 m and 120 m resolutions — pixel scales at which the source area influencing the tower measurement (~100 m) is reasonably resolved. At 960 m, the agreement is relatively poor, especially for the latent heat flux, due to sub-pixel heterogeneity in land surface conditions at scales exceeding the tower footprint. Therefore in this particular landscape, thermal data at 1-km resolution are not useful in assessing the intrinsic accuracy of the land-surface model in comparison with tower fluxes. Furthermore, important spatial patterns in the landscape are lost at this resolution. Currently, there are no definite plans supporting high resolution thermal data with regular global coverage below ~700 m after Landsat 5 and ASTER fail. This will be a serious problem for the application and validation of thermal-based land-surface models over heterogeneous landscapes.
Published by Elsevier Inc.

Keywords: Remote sensing; Spatial resolution; Land surface flux; Footprint

1. Introduction

Remote sensing-based land surface models have demonstrated ability to provide spatially distributed estimates of energy fluxes/evapotranspiration (ET) over large areas (e.g., Diak et al., 2004). However, the ability to capture the full range of variability in the fluxes is dependent on the resolution of the remote sensing data. For example, in a relatively homogeneous cropping region in Iowa where over 90% of vegetation cover is either corn or soybean, Kustas et al. (2004a) found that when the resolution is >500 m, fluxes from the two crops could not be easily distinguished. Clearly, for landscapes with significant variability in vegetation cover, type/architecture, and moisture, the spatial resolution of the remote sensing data is crucial for discriminating fluxes for the different land cover types and hence avoiding significant errors due to application of a land surface model to a mixed pixel containing large contrasts in surface temperature and vegetation cover (Kustas & Norman, 2000a; Moran et al., 1997).

Operationally, many applications in the western U.S. require assessment of ET variability at high spatial resolutions of 10^2 m and finer. To accurately characterize ET or moisture stress for even a single relatively large agricultural field (~500×500 m),

* Corresponding author. Tel.: +1 301 504 7614; fax: +1 301 504 8931.
E-mail address: Fuqin.Li@ars.usda.gov (F. Li).

0034-4257/$ - see front matter. Published by Elsevier Inc.
doi:>10.1016/j.rse.2006.11.032

for example, there needs to be several within-field pixels to allow averaging and to clearly distinguish contributions from adjacent fields. Water managers must account for evaporative losses along canals and riparian corridors ($\sim 10^1$–10^2 m wide) in planning for water distribution within irrigation districts. Moreover, to properly validate remote sensing land surface models, the model grid must resolve the surface footprint of the flux measurement device, which is typically a tower-based eddy covariance system with a source-area/flux-footprint of a few 100 m or less. For grids coarser than the measurement footprint, model-measurement differences over heterogeneous landscapes will not necessarily be representative of the intrinsic model accuracy (Anderson et al., 2004).

Current operational thermal sensors are at relatively coarse resolution (~1 km for MODIS — Moderate Resolution Imaging Spectroradiometer), making it difficult to account for the spatial variation in fluxes for many landscapes. Unfortunately, it also is not certain whether future Landsat programs will support a high resolution (~100 m) thermal band sensor. The main objective of this paper is to determine if and how restriction to MODIS-resolution thermal data will limit our ability to apply and validate remote-sensing-based energy balance models over heterogeneous surfaces.

To investigate the impact of model/remote sensing resolution on flux estimation, three Landsat 5 Thematic Mapper (TM) scenes collected during the 2004 Soil Moisture Experiment (SMEX04) conducted in southern Arizona and Mexico were combined with local meteorological measurements to drive simulations from a remote sensing-based land surface model during the dry and wet/monsoon seasons. We focus on three landscapes featuring different types of spatial structure: two upland sites, one with grass cover and patches of shrubs correlated with the terrain and the other with relatively uniform sparse shrubland cover; and a riparian site near the San Pedro River. The impact of resolution on variability in model land surface fluxes is examined for these semiarid heterogeneous landscapes, where 1-km pixels may represent a mixture of relatively low evapotranspiration for the upland areas and high values from the riparian corridor.

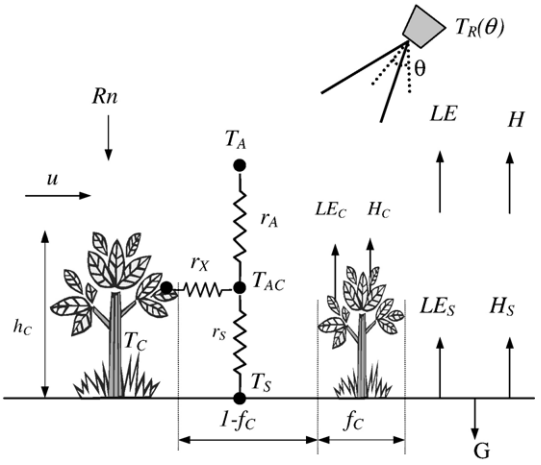

Fig. 1. Schematic diagram illustrating the resistance network for the TSM. Also shown are the flux partitioning between soil (subscript S) and canopy (subscript C) and key model inputs. Symbols are defined in the text.

2. The model

The model used in this study is the series version of the Two-Source-Model (TSM) developed by Norman et al. (1995). The formulations presently used in the TSM are described in Kustas and Norman (1999), and more recently in Li et al. (2005), with the resistance network and modeling framework illustrated in Fig. 1. In the TSM, the key remotely sensed variables are radiometric surface temperature (T_R) and vegetation cover fraction (f_C). The model partitions T_R between the vegetation and soil components within the scene, weighted by f_C:

$$T_R(\theta) \approx [f_C(\theta) T_C^4 + (1 - f_C(\theta)) T_S^4]^{1/4} \quad (1)$$

where T_C is canopy temperature, T_S is soil temperature and $f_C(\theta)$ is the fractional vegetation cover at the thermal sensor view angle θ.

The sensible heat flux (H) is also partitioned between the vegetated canopy (H_C) and soil (H_S):

$$H = H_C + H_S = \rho C_P \frac{T_{AC} - T_A}{r_A} \quad (2)$$

$$H_C = \rho C_P \frac{T_C - T_{AC}}{r_X} \quad (3)$$

$$H_S = \rho C_P \frac{T_S - T_{AC}}{r_S} \quad (4)$$

where ρC_P is the volumetric heat capacity of air ($Jm^{-3}\ K^{-1}$), T_{AC} is the air temperature in canopy-air space, T_A is the air temperature, r_A is the aerodynamic resistance to heat transfer across the canopy-surface layer interface (Kustas & Norman, 1999), r_X is the total boundary layer resistance of the complete canopy of leaves (see Kustas & Norman, 1999) and r_S is the resistance to heat flow in the boundary layer immediately above the soil surface (see Kustas & Norman, 1999). In the current application of the model, both T_A and $T_R(\theta)$ are from the observations (i.e., T_A from the on-site flux tower and $T_R(\theta)$ from Landsat thermal observations), whereas T_S, T_C and T_{AC} are computed by the TSM. The resistance terms r_X, r_A and r_S are largely influenced by vegetation properties, wind speed and atmospheric stability (see Kustas & Norman, 1999; Kustas et al., 2004b; Norman et al., 1995).

The latent heat flux from the vegetated canopy (LE_C) is initially computed from the Priestley–Taylor formulation:

$$LE_C = \alpha_{PT} f_G \frac{\Delta}{\Delta + \gamma} Rn_C \quad (5)$$

where γ is the psychrometric constant ($\approx 67\ PaK^{-1}$), Δ is the slope of the saturation vapor pressure verses temperature curve, α_{PT} is Priestley–Taylor parameter (~1.3), f_G is the fraction of the leaf area index (LAI) that is green, and Rn_C is divergence of net radiation within the vegetative canopy layer is described by Kustas and Norman (1999, 2000b).

The surface soil heat flux (G) is estimated as a fraction of net radiation just above soil surface, Rn_S

$$G = C_G Rn_S \quad (6)$$

where $C_G \sim 0.35$, and has been expressed as a function of time to accommodate known temporal variation in this "constant" (Santanello & Friedl, 2003).

With the above system of equations, energy conservation for the canopy component ($Rn_C = LE_C + H_C$) and for the soil ($Rn_S = LE_S + H_S + G$), and the initial assumption of unstressed conditions, a solution for both the thermal/radiation balance and the turbulent heat fluxes for the soil and canopy components can be achieved. More details on model convergence and methodology for computing fluxes under stressed vegetation conditions where Eq. (5) is not valid are discussed in Kustas et al. (2004b).

It is important to point out that the TSM was developed to deal with partial canopy cover conditions and that it has greater utility than most other remote sensing-based land surface models that do not consider differences in soil and canopy contributions to the radiative temperature and convective/energy exchanges (Norman et al., 1995). Single-source models that do not explicitly treat the difference between the soil and canopy exchange coefficients (resistances), r_S and r_X, often require empirical bulk "extra resistance" factors to reproduce measured sensible heat fluxes, especially in dry, arid regions with sparse vegetation (e.g., Stewart et al., 1994; Verhoef et al., 1997).

3. Data and methods

3.1. Site and field experiment description

SMEX04 was conducted in southern Arizona and Mexico during the July to August monsoon season of 2004. This paper focuses on a study area in Arizona that includes an upland dry region where most vegetation is shrub and grass with 20% to 40% cover and a relatively wet riparian area where most vegetation is mesquite forest with cover fraction ranging between 60% and 90%. The climate is classified as semi-arid with mean annual precipitation around 400 mm. During the

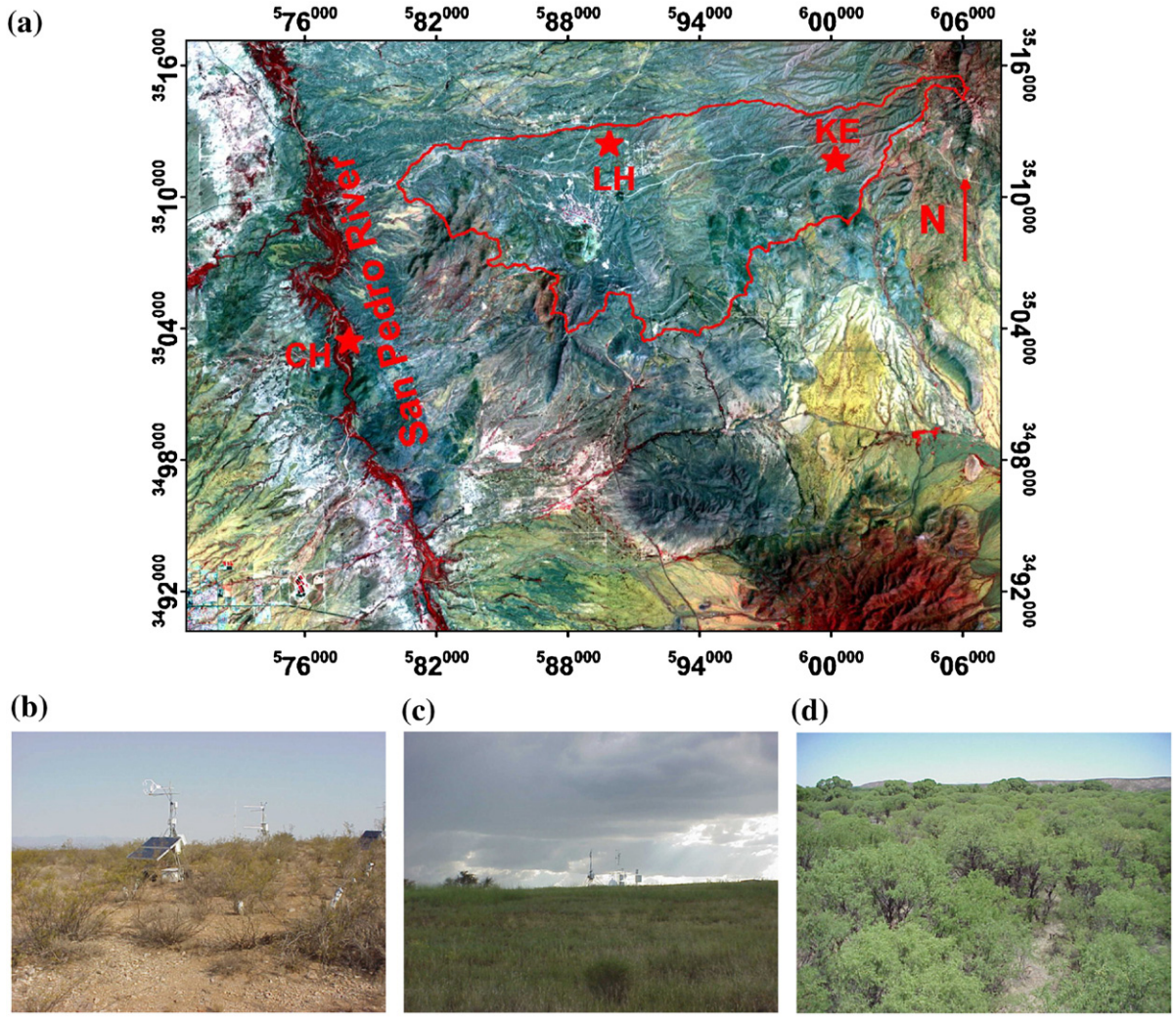

Fig. 2. Approximate location and local surface conditions of the three tower sites operating during SMEX04 where (a) is a Landsat false color image with three tower location noted, LH is Lucky Hills, KE is Kendall and CH is Charleston, and photos of the (b) Lucky Hills, (c) Kendall and (d) Charleston tower sites.

experiment, two eddy covariance flux towers were operating in the upland areas: one in a shrubland subwatershed (Lucky Hills, 31.744° N Lat./110.052° W Long.) and another in a grassland subwatershed (Kendall, 31.737° N Lat./109.942° W Long.). Both episodic surface energy balance measurements (Stannard et al., 1994) and longer term observations (Emmerich, 2003) have been conducted at these subwatersheds prior to SMEX04. The other flux tower was located in a riparian woodland site (Charleston 31.664° N Lat./110.178° W Long.) east of the San Pedro River and has observations spanning over several years (Scott et al., 2004). In addition to the energy fluxes, the towers provided measurements of local meteorological conditions, including solar radiation, air temperature, vapor pressure and wind speed, all used as input for the TSM scheme.

In Fig. 2, a Landsat false color image shows the USDA-ARS Walnut Gulch Experimental watershed boundary, a key test site for past interdisciplinary field experiments in this region (Goodrich et al., 2000; Kustas and Goodrich, 1994), and the approximate locations of the three eddy flux towers. In addition, a photo taken at each of the flux tower locations is shown, providing a qualitative assessment of the vegetation conditions for these sites. The Lucky Hills site at an elevation of ~1370 m above mean sea level (amsl) had the lowest vegetation cover at ~25%, on average, consisting primarily of ~1 m tall mesquite shrub. The Kendall subwatershed at an elevation of ~1531 m amsl is predominately upland grassland with ~40% cover and ~0.3 m canopy height, on average. The Charleston site at 1199 amsl is located in a riparian mesquite forest having ~7 m tall vegetation at roughly 75% cover. Fractional vegetation cover conditions have significant spatial variability and are strongly influenced by climatic factors, namely the duration of the dry season and amount and duration of rainfall during the wet or monsoon season. A summary document of the SMEX04 project can be accessed via the web at http://www.ars.usda.gov/Research/docs.htm?docid=8995.

Land cover/land use information and vegetation cover fraction fields for a ~3×3 km area encompassing each flux tower site are shown in Fig. 3. The f_C fields are computed using the Normalized Difference Vegetation Index (NDVI; see Sec. 3.3) derived from Landsat 5 images collected on June 11 during the dry season and on July 29 during the "monsoon" or wet season (see below). Between the June and July overpasses there

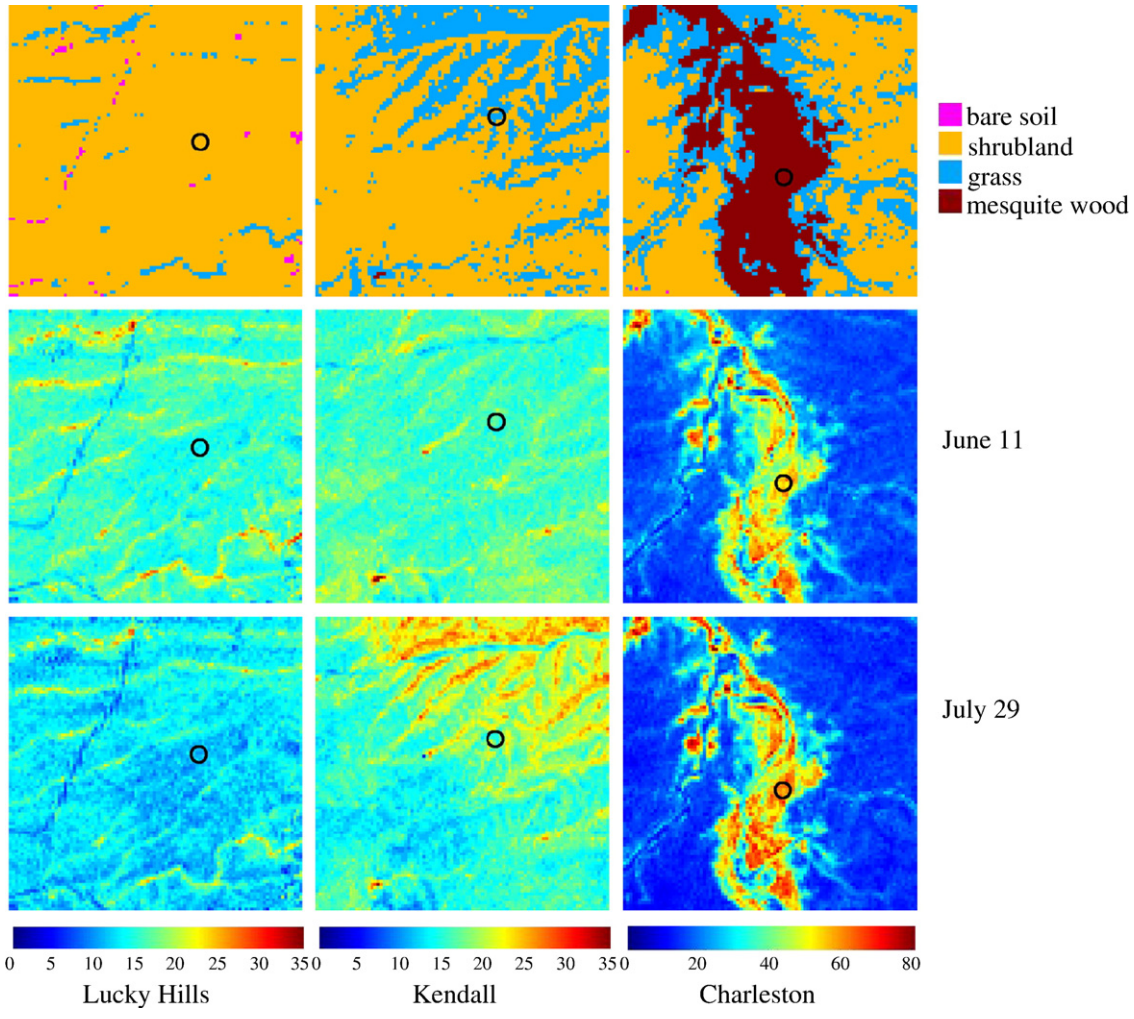

Fig. 3. Land cover/land use and percentage vegetation cover fraction (%) maps (30 m resolution) for a ~3×3 km area encompassing the Lucky Hills, Kendall and Charleston tower sites for the June 11 (dry season) and July 29 (monsoon season) 2004 Landsat 5 overpass dates.

is a "green up" particularly for the Kendall site and the grassland cover type as well as for areas along the riparian corridor for the Charleston site. For Lucky Hills, which is almost uniformly shrubland, there is no significant change in f_C. The slight decrease in f_C observed at Lucky Hills falls within the expected errors related to the atmospheric correction of the NDVI bands, and hence may not truly reflect actual changes in vegetation cover conditions. Rain gauge observations for June and July prior to the July 29 overpass indicated that the Kendall site received 63 mm of rain compared to only 22 mm at Lucky Hills, which may help explain the lack of any measurable increase in green vegetation at the Lucky Hills site.

The differences in the vegetation cover/land use and vegetation cover/greenness patterns will have a significant effect on the model results. For Kendall and Lucky Hills, the spatial patterns of low and high evaporative flux correlate with the local topography, where dissected ephemeral channels generally support larger vegetation having deeper rooting systems, while the drier ridges have less available root-zone moisture and hence have lower vegetation cover. The only caveat to this is during the monsoon season where more frequent precipitation can support the green-up of vegetation (grasses primarily) wherever they exist in the landscape. For the Charleston site, the available water along the San Pedro River amplifies the difference in the amount and size of vegetation cover with the drier upland areas.

3.2. Micrometeorological data

Local meteorological data required by the model – namely solar radiation, air temperature, vapor pressure, and wind speed and direction – were acquired with instrumentation mounted on the flux towers several meters above the canopy. In addition, each tower was equipped with an infrared thermometer (IRT) to measure radiometric surface temperature. The tower-based radiometer data were used to interpret and validate the atmospheric correction of the Landsat surface temperature imagery.

The flux towers were also equipped with instruments measuring net radiation, soil heat flux, as well as sensible, latent, momentum and CO_2 flux using the eddy covariance (EC) technique. The 3-dimensional sonic and fast response water vapor/CO_2 sensors were maintained at a minimum nominally two times the canopy height (i.e., $2h_C$) to minimize roughness sublayer effects. Measurement heights for the EC sensors used in the present study were at approximately 3 m above local topography at Lucky Hills, 2 and 10 m at Kendall (Kendall site had two eddy covariance sensor systems) and 13 m at the Charleston site. The instrument set-up and measurement system/design for all three sites were similar with corrections to the raw eddy covariance data following the procedures summarized in Scott et al. (2004).

As is the case with most study sites employing the eddy covariance technique, there is a general lack of energy balance closure among the flux measurements (Twine et al., 2000). Possible causes for closure residuals include instrumental effects, post-processing corrections applied to the turbulence data, the length of the sampling interval, and the heterogeneity of the landscape, just to name a few (Foken et al., 2006). For the flux observations during the Landsat overpass times, a comparison of available energy $Rn-G$ versus the turbulent fluxes $H+LE$ indicates a closure residual of ~80 W m^{-2} on average (Fig. 4). This translates to approximately a closure ratio $(H+LE)/(Rn-G)$ of ~80%, similar to results found for the Ameriflux sites (Wilson et al., 2002). Since the TSM requires energy conservation, closure in the flux measurements was enforced through a residual method; that is, LE for the tower measurements was recalculated as the residual of the surface energy budget, namely $LE_{RE}=Rn-G-H$. Although this assumes measurement errors are entirely in LE, there are a few studies that suggest EC measurements tend to be more problematic for latent heat than for sensible heat (Li et al., 2005).

3.3. Remote sensing data

During the SMEX04 field campaign, three Landsat TM scenes were collected over the experiment area. As mentioned earlier (see Fig. 3), one scene was acquired during the dry season on June 11, 2004 and other two were obtained during the wet monsoon season on July 29, 2004 and August 30, 2004, respectively. The Landsat images were used to derive land-use classifications, fractional vegetation cover and LAI, and radiometric surface temperature (T_R) over the study sites using atmospheric correction techniques described by Li et al. (2004). Fractional cover was obtained from the NDVI using a relationship suggested by Choudhury et al. (1994):

$$f_C = 1 - \left(\frac{NDVI_{max} - NDVI}{NDVI_{max} - NDVI_{min}}\right)^a \quad (7)$$

where a is a function of canopy architecture, but for most vegetation is typically set equal to 0.7, and $NDVI_{max}$ and $NDVI_{min}$

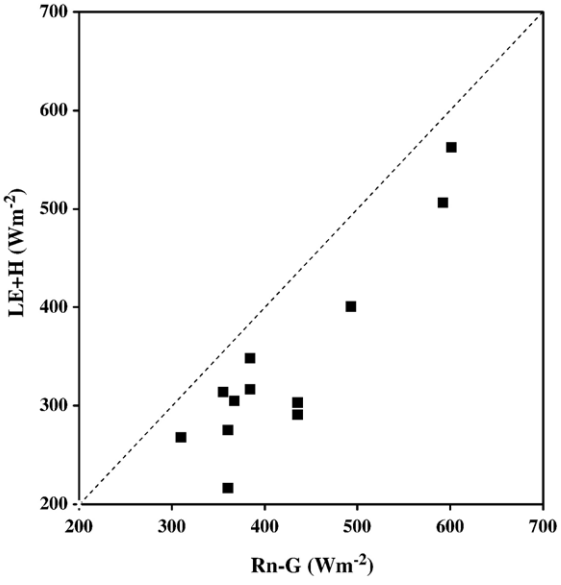

Fig. 4. Comparison of the sum of the measured turbulent fluxes ($H+LE$) from the eddy flux towers versus the available energy ($Rn-G$) for assessing energy balance closure. Dashed line represents perfect agreement.

represent typical values associated with full vegetation cover and bare soil, respectively. For the study dates, Eq. (7) yields vegetation cover fraction estimates on the order of 10–15 % over Lucky Hills, ~20–25% at Kendall and ~55–65% for the Charleston site — slightly lower than the nominal values typically associated with these sites; this may be due to a drier than normal conditions during the 2004 monsoon season. The LAI was estimated using the following formulation (Choudhury, 1987):

$$\mathrm{LAI} = -\frac{\ln(1-f_C)}{0.5} \tag{8}$$

Apparent cover fraction at view angle ϕ is then obtained with

$$f_C(\theta) = 1 - \exp\left(\frac{-0.5\Omega(\theta)\mathrm{LAI}}{\cos(\theta)}\right) \tag{9}$$

where $\Omega(\theta)$ is a directional clumping factor used to consider the effect of clumped vegetation, which exists in many row crops and natural landscapes (Anderson et al., 2005; Kustas & Norman, 2000b). The directionality of $\Omega(\theta)$ depends on canopy architecture, as specified in Kustas and Norman (1999).

Atmospheric corrections to the at-satellite brightness temperatures were estimated with the MODTRAN 4.1 radiative transfer model (Berk et al., 1998), using radiosonde atmospheric profiles of pressure, temperature and water vapor obtained from nearby Tucson meteorological station (station number 23160, 32.12 N and 110.93 W, elevation 788 m) with a correction for the difference in mean elevation between the towers and meteorological station site. The derived TM surface brightness temperatures were compared with tower-based IRT observations taken at Lucky Hills, Kendall, and Charleston (Fig. 5), yielding a root-mean-square difference (RMSD) of 1.55 °C. This suggests that relatively accurate atmospherically-corrected surface temperatures were derived from the Landsat

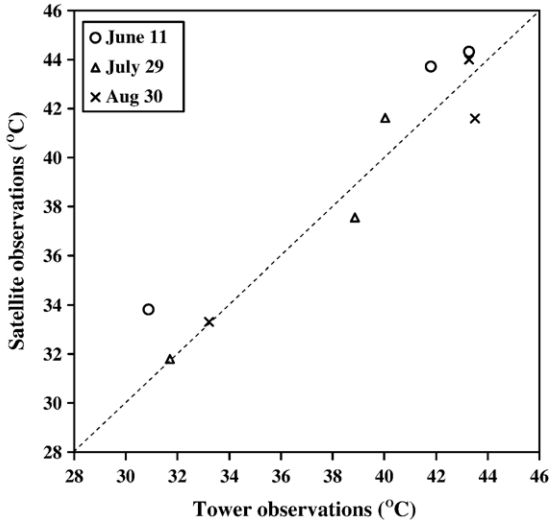

Fig. 5. Comparison of Landsat versus ground-based surface brightness temperatures for the three flux tower sites on the overpass days. Dashed line represents perfect agreement.

Table 1
Values of key TSM inputs and parameters for the three main land cover classes in the Walnut Gulch experimental site

Land cover	h_C (m)	w (m)	$\Omega(0)$ (–)	α_{PT} (–)	f_G (–)
Grass	0.3	0.01	0.8	1.3	1
Shrub	1	0.05	0.8	1.3	1
Mesquite forest	7	0.05	1	1.3	1

h_C: canopy height.
w: leaf width.
$\Omega(0)$: nadir clumping factor.
α_{PT}: Priestley–Taylor parameter.
f_G: fraction of green vegetation.

thermal imagery. To convert brightness temperature to radiometric temperature, surface emissivity was estimated by weighting the estimated soil and vegetation emissivities by the local fractional cover, namely $\varepsilon_\lambda \approx \varepsilon_C f_C + (1-f_C)\,\varepsilon_S$ where ε_λ is the composite emissivity, ε_C is the vegetated canopy emissivity, ε_S is the soil emissivity (Li et al., 2004). Values of ε_C and ε_S are assigned as 0.994 and 0.959, respectively according to emissivity measurements conducted by Humes et al. (1994) for this region.

3.4. Model inputs and variable/parameter values

Table 1 lists the key model variable/parameter values assigned to the main land cover types: grassland, shrubland and mesquite forest. With nominal canopy height, h_C estimated from land cover information and prior ground surveys, the aerodynamic roughness, z_O and displacement height, d_O are computed using simple ratio-based formulas, namely, $z_O/h_C = 0.1$ and $d_O/h_C = 0.67$. Other model variables, including Priestley–Taylor parameter α_{PT} and fraction of green vegetation f_G, were assigned the default values of 1.3 and 1, respectively. A nominal value for the nadir clumping factor, $\Omega(0) = 0.8$ for the shrubland and grassland and $\Omega(0) = 1$ for the riparian mesquite woodland was assigned based on prior applications of the TSM for this landscape (Kustas & Norman, 2000a). It should be noted that there was no *a priori* calibration of any of the TSM parameters/variables, and hence the same values or formulations used for the SMEX04 site were the same as those used for SMEX02 site (Li et al., 2005) having very different climate and vegetation conditions (corn and soybean production region in central Iowa).

Meteorological inputs to the TSM at the tower sites for the three Landsat overpass dates are listed in Table 2. The Kendall site tends to have the lowest air temperature and highest wind speed observations due to its high elevation and high sensor location (using 10 m observations) relative to the top of the canopy (see Table 1). Differences in sensor heights between tower locations are accommodated in the resistance formulations for r_X, r_A and r_S (Norman et al., 1995).

3.5. Data processing and analyses

3.5.1. Generation of multi-resolution satellite datasets

Remote sensing data at three different spatial resolutions were employed to test the effect of input resolution on TSM flux

Table 2
Meteorological inputs to the TSM for the Landsat 5 imaging dates during SMEX04

Flux tower site	Overpass date	u (m s^{-1})	T_A (C)	e_A (kPa)	R_S (W m^{-2})
Lucky Hills	June 11	2.0	26.2	0.32	968
Kendall	June 11	3.4	23.7	0.27	992
Charleston	June 11	2.1	25.6	0.47	961
Lucky Hills	July 29	4.2	28.2	1.13	882
Kendall	July 29	5.2	25.6	1.18	913
Charleston	July 29	3.0	28.5	1.56	875
Lucky Hills	August 30	1.5	29.8	0.99	832
Kendall	August 30	1.7	27.7	0.95	872
Charleston	August 30	1.5	30.1	1.38	846

u: wind speed.
T_A : air temperature.
e_A: vapor pressure.
R_S: incoming solar radiation.

predictions: the 30 m resolution of the Landsat visible and near-infrared (vis/NIR) bands, the 120 m resolution of the Landsat 5 thermal band, and 960 m, which is the nominal resolution of the thermal band on MODIS. These resolutions span a range in length scales inherent in the variability in landscape features for this semiarid region, and also a range of current instrumental resolutions associated with thermal remote sensing in native and processed forms.

Thermal data at 30 m were bi-linearly interpolated from the native 120 m resolution of the Landsat 5 thermal sensors and co-registered with the vis/NIR band data — the standard data format provided by the U.S. Geological Survey. While a more rigorous technique described by Kustas et al. (2003) could have been employed to spatially sharpen the thermal imagery to the vis/NIR band resolutions, exploiting the natural correlations that exist between surface temperature and vegetation indices for many landscapes, Agam et al. (2007) demonstrate that improvements in retrieval accuracy using sharpening are only on the order of 1 °C at the higher resolutions.

At 30-m resolution, fine detail in vegetation cover patterns associated with topographic and water-body features can be detected. In moving up to the 120-m native resolution of Landsat 5, we can examine whether model validation significantly deteriorates and significant spatial contrast is lost. This is important to investigate since ~100 m is suggested as the highest resolution for any thermal sensors that may be on the next Landsat platform. Finally, 960-m resolution images were created by uniformly aggregating the 120-m data to represent the current operational thermal data available from MODIS. At this resolution, we investigate the degree to which spatial variation in modeled fluxes is lost and how model validation using tower-based measurements is compromised due to the significant mismatch in pixel resolution (~1000 m) versus size of source-area/flux-footprint (~100 m).

3.5.2. Application of two-dimensional source-area footprint model

A two-dimensional footprint model was used to estimate the source area on the land-surface contributing to the eddy flux measurements, and associated pixel weights used in integrating gridded TSM fluxes to the observation footprint scale. The model is based on Hsieh et al.'s (2000) one-dimensional model, including a lateral dispersion formulation to simulated distributions in the cross-wind dimension (Detto et al., 2006). The basic equation for the along-wind footprint model (estimating upwind source contributions) can be expressed as:

$$f(x,z_m) = \frac{1}{k^2x^2} DZ_U{}^P |L|^{1-P} e^{\frac{-DZ_U{}^P|L|^{1-P}}{k^2x}} \quad (10)$$

where L is the Obukhov length, D and P are similarity constants with different values for unstable, neutral and stable atmospheric conditions (see Hsieh et al., 2000), x is the fetch in the upwind direction, k is von Karman's constant, and Z_U is a length scale given by

$$Z_U = z_m(\ln(z_m/z_O) - 1 + z_O/z_m) \quad (11)$$

where z_m is flux observation height and z_O is the surface roughness for momentum.

If lateral dispersion is added to the above footprint model, then a 2-D source area function is generated. The 2-D footprint model can be expressed as:

$$f(x,y,z_m) = \frac{1}{\sqrt{2\pi}\sigma_y} e^{-0.5\left(\frac{y}{\sigma_y}\right)^2} f(x,z_m) \quad (12)$$

where the standard deviation σ_y can be related to the standard deviation in the lateral wind fluctuations as (Eckman, 1994)

$$\sigma_y = a_1 z_O \frac{\sigma_v}{u*} \left(\frac{x}{z_O}\right)^{p_1} \quad (13)$$

where σ_v is the standard deviation of the cross wind velocity, u_* is the friction velocity, and typical values for the model parameters are $a_1 = 0.3$ and $p_1 = 0.86$. A schematic illustration of a typical flux footprint generated by this code is shown in Fig. 6 using tower measurements from the Kendall site for July 29.

In the comparisons shown below between modeled and measured fluxes, the gridded model output has been integrated

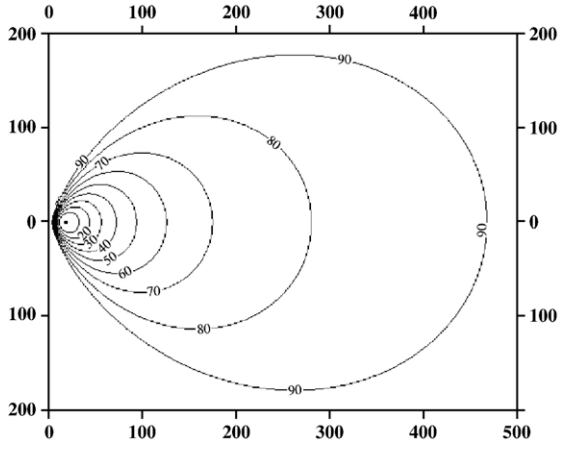

Fig. 6. Schematic illustrating two-dimensional footprint model prediction of weighted source-area contribution. Horizontal and vertical scales are in meters. The circular isolines represent cumulative flux in percentage. Footprint model output using 10 m height sensor measurements from Kendall on July 29, 2004.

as a weighted sum output over the tower source area $(\overline{\mathrm{FLUX}})$ via the following expression:

$$\overline{\mathrm{FLUX}} = \frac{\sum_{i=1}^{n} f(x_i, y_i, z_m)\mathrm{FLUX}(x_i, y_i)}{\sum_{i=1}^{n} f(x_i, y_i, z_m)} \quad (14)$$

where i indicates a pixel in the model grid at location x_i, y_i. Note that the ability to resolve the footprint is degraded at coarser model grid scales.

4. Results

4.1. Spatial variability in modeled flux as a function of resolution

In Fig. 7, the spatial patterns in latent heating as computed by the TSM are illustrated for the ~3×3 km (more precisely 2.88×2.88 km) grids surrounding each of the tower locations at the three resolutions. Fields of LE are shown for two days; one representative of the dry season (June 11, 2004) and the other showing conditions typical of the monsoon season (July 29,

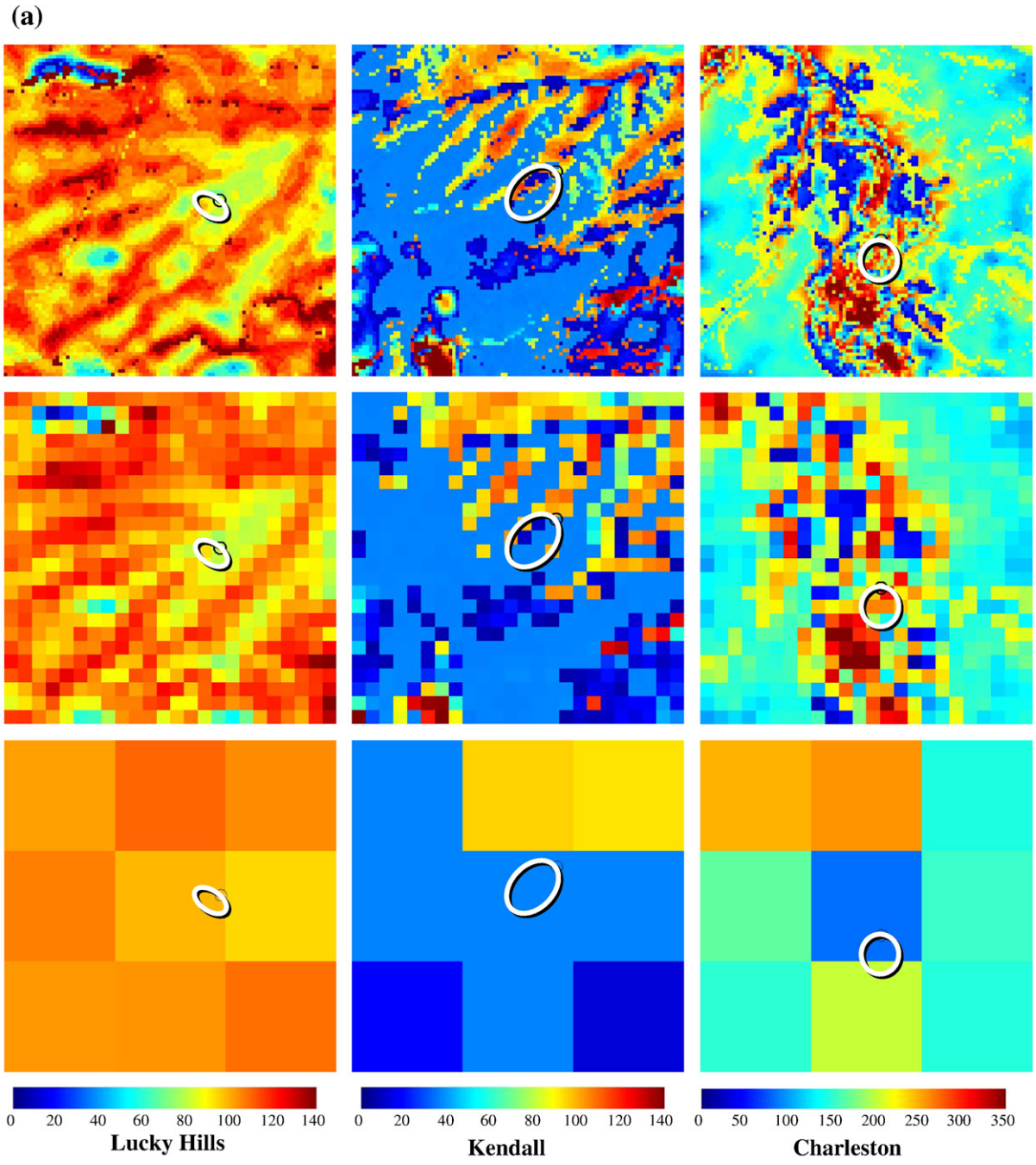

Fig. 7. Spatial distribution of LE (W m^{-2}) computed for a ~3×3 km area surrounding the three tower locations for the (a) dry season overpass, June 11, 2004 (b) for one of the monsoon season overpasses, July 29 2004. The oval shaped areas outlined in white represent upwind two-dimensional source area patches contributing to the tower eddy flux measurements estimated via Eq. (12).

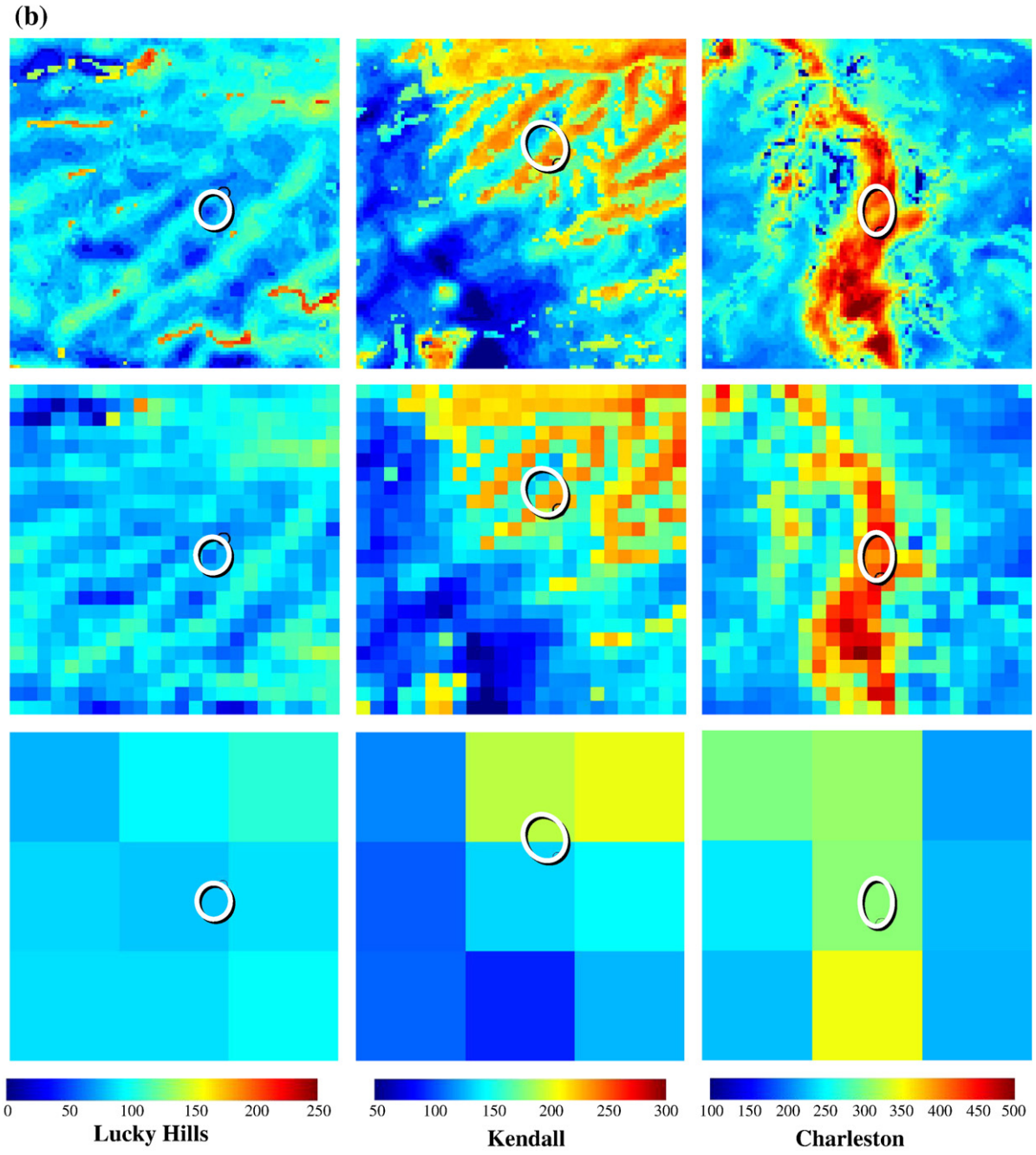

Fig. 7 (*continued*).

2004), after rains caused the landscape to green up (see also Fig. 3). Also illustrated on these images is the approximate source-area footprint upwind of the EC tower, as estimated by Eq. (12). The size of the footprint in each case depends on sensor height, local roughness and wind speed/stability conditions.

The high resolution output from the TSM (30 m) shows significant spatial variability, especially around the Charleston site where the latent heat flux ranges between 100 and 500 W m^{-2} for the image during the monsoon season. Although some spatial information is lost at the 120 m resolution, the general patterns and range in magnitudes in LE are preserved. At 960 m resolution, however, the variability in LE is dramatically reduced, and the spatial structures in the landscape are obscured. In most cases at 960 m, the flux footprint is encompassed in a single pixel; consequently, there is no differential weighting of the high-resolution structure in LE observed at the Charleston and Kendall sites. At Lucky Hills, the relatively uniform distribution of shrubs and other vegetation cover creates a relatively homogeneous pattern in LE at the 10^1–10^2 m scale. The Kendall site shows greater spatial variation in latent heating reflecting spatial patterns in land cover (grassland versus shrubs), particularly for the July 29 overpass (see Fig. 3). The Charleston site, which includes both riparian mesquite forest and upland desert shrubs and grasses, exhibits the greatest spatial variation in LE. Unfortunately, a

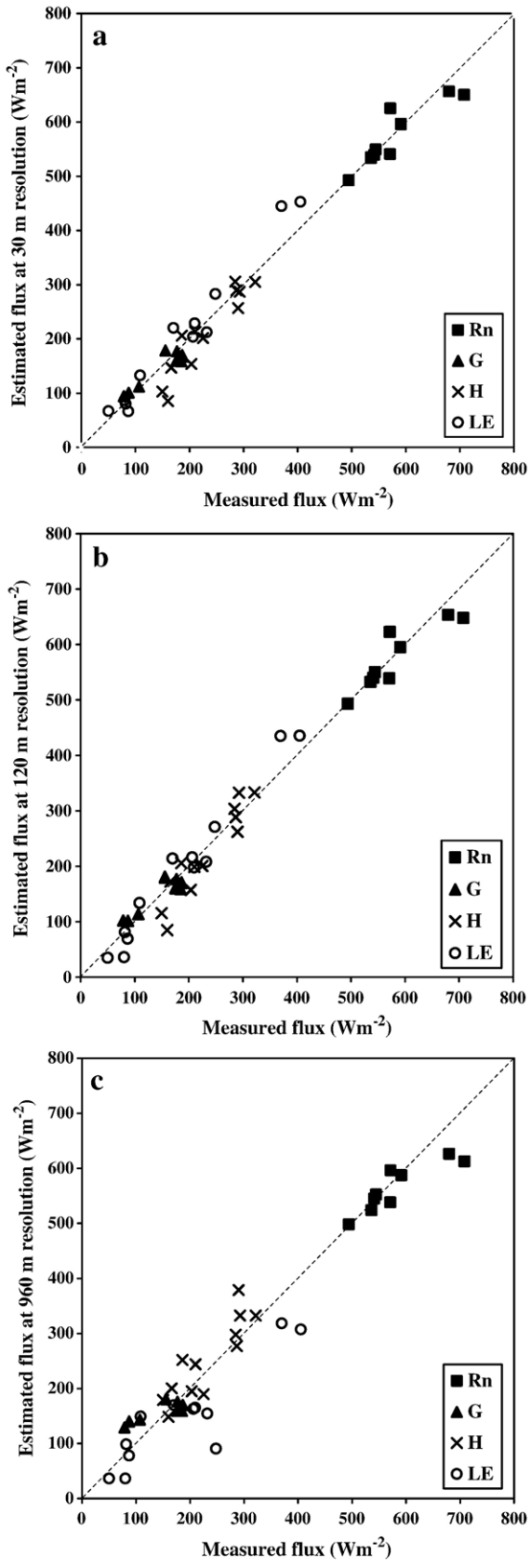

Fig. 8. Comparison between flux tower observations and TSM modeled output at different resolution scales: a) 30 m, b) 120 m, c) 960 m. Note *LE* is adjusted to ensure closure by the residual method, LE_{RE} (see text for details). Dashed line represents perfect agreement.

semivariogram analysis of spatial structure in the TSM flux fields, as performed by Kim et al. (2006), could not be conducted with these datasets due to the relatively large pixel size (30 m) compared to the length scales of variability in canopy cover (plant spacing) and other important surface states and landscape features, which were on the order of 1–10 m (Moran et al., 1997). Hence it was not possible to resolve important structures, such as the range, in the semivariogram.

With the higher resolution data (30 and 120 m), the TSM can even detect vegetation stress (patches with low LE) around the riparian site (Charleston) during the dry season (compare Fig. 7a and b). Stress can occur here when there is a prolonged drought and the riparian vegetation has exhausted available water deeper in the soil profile. Patches of grass and smaller shrubs that exist within the riparian corridor would be most susceptible to drought during the dry season due to shallow rooting depths in comparison with the taller mesquite trees (see Fig. 3). With the 960-m resolution data, the TSM is unable to detect stressed conditions unless they cover a significantly larger area of the landscape.

4.2. Model validation

4.2.1. High resolution

Comparison of the TSM output using the high (30 m) resolution data versus tower-based fluxes yields relatively close agreement (see Fig. 8a) with root mean square difference (RMSD) values between 20 and 35 W m^{-2} (see Table 3). These RMSD values are similar to results obtained by Li et al. (2005) applying the TSM with Landsat data over a corn and soybean production region in central Iowa during SMEX02. Significantly greater discrepancies (RMSD ~100 W m^{-2}) are obtained between modeled and measured LE without closure at all three resolutions. This artificial inflation of model-measurement differences is mainly due to the relatively large magnitude of the closure residual (~80 W m^{-2}) causing a significant bias between modeled and measured LE, as has been observed in other studies (e.g., Crow et al., 2005; Li et al., 2005). However, since TSM requires energy conservation, a requisite condition for any energy balance model, to maintain consistency the measurements need to also conform to this physical constraint (Twine et al., 2000).

The fact that the TSM can be applied to both arid and humid climatic regions supporting very different vegetation types (crops versus natural vegetation), cover and density, yielding similar results with no *in situ* model calibration of extra

Table 3
Difference statistics (RMSD) comparing flux tower measurements and TSM estimates of net radiation, (Rn), soil heat flux (*G*), sensible heat flux (*H*) and latent heat flux (LE) at three different pixel resolutions

Resolution (m)	Rn (W m^{-2})	*G* (W m^{-2})	*H* (W m^{-2})	LE_{RE} (W m^{-2})
30	27	18	33	34
120	27	18	33	32
960	36	29	40	69

Note that model-measurement comparisons for LE are made with forcing closure by residual for the eddy covariance data.

resistance parameters provides strong evidence of the robustness of the TSM formulation. Moreover, although TSM uses the Priestley–Taylor approximation as an initial guess for the canopy transpiration flux, which may not seem appropriate for the semi-arid climate of Arizona, the system latent heat fluxes predicted by the model are quite reasonable. The model has a built-in mechanism for throttling α_{PT} back from its potential value when conditions of vegetation stress are detected (Kustas et al., 2004b). For the June 11 overpass, during the dry season when stress might be expected, the TSM predicted a decrease in the α_{PT} value from 1.3 to ~0.75 for the Kendall site and to ~1.1 for the Charleston site (average for the estimated flux footprint/source-area), while Lucky Hills site having relatively low cover, did not require a reduction in the α_{PT} value. The general utility of the TSM for a wide variety of environmental conditions and landscape properties has been supported in earlier studies using ground-based T_R observations, particularly when compared to other thermal-based models that do not explicitly parameterize soil and vegetation temperatures and energy exchange (e.g., Zhan et al., 1996).

4.2.2. Resolution effects

Model output at 30, 120 and 960-m resolution is compared to the flux measurements from the three flux tower sites in Fig. 8a, b, and c, respectively, with RMSD values tabulated in Table 3. The results in Fig. 8a and b indicate that both the 30 and 120-m resolution output from the TSM is in good agreement with the tower flux measurements when the energy budget residual correction is applied to the latent heating observations (LE_{RE}). However, when the resolution is degraded to that of the MODIS thermal band, the agreement with observations deteriorates, especially for the turbulent fluxes LE and H (Fig. 8c) and for the Charleston site in particular, represented by the points furthest from the 1:1 line in Fig. 8c.

At 960-m resolution, pixels are invariably a mixture of vegetation types and cover fractions. This is particularly the case for the Charleston site, where the width of the riparian zone is typically on the order of 50 to 500 m. Consequently, with such coarse resolution it is impossible to capture a representative range in LE over the riparian area. Furthermore, since according to the footprint model 90% of the upwind source-area affecting the eddy flux measurements was within 500 m of the tower, with peak contributions occurring within 100 m, there is a serious mismatch between the model-measurement resolutions at the MODIS thermal pixel scale (Figs. 6 and 7). The footprint is well-resolved at 30 m, and marginally resolved at 120 m, so high-resolution structure in the surface flux patterns influencing EC observations can be captured reasonably at these resolutions. Using the thermal sharpening technique of Kustas et al. (2003), 1-km thermal images from MODIS could be sharpened to the 250 m resolution of the MODIS NDVI product. However for standard flux tower measurements collected a few meters above the canopy under typical daytime convective conditions, the footprint model indicates that 250 m T_R data are still too coarse to capture any significant flux variability within the source-area/flux-footprint.

The statistical results listed in Table 3 support these conclusions regarding optimal resolutions for model validation. The RMSD between modeled and measured LE, for example, is similar for the 30 and 120-m resolution simulations (~30 W m^{-2}) but is nearly double at 960-m resolution (~70 W m^{-2}). Clearly, a meaningful assessment of intrinsic model accuracy is not possible when there is significant spatial variability in surface conditions and fluxes at length scales an order of magnitude less than the resolution of the key remotely sensed inputs to the land surface model.

In Fig. 9, TSM estimates of the turbulent fluxes at the high (30 m) resolution integrated over the source-area footprint (Eq. (14)) are compared with fluxes from the low resolution (960 m) simulation in the pixel encompassing the tower site (at that scale, the extent of the source area lies within a single pixel). This comparison clearly shows that, for certain landscapes, the TSM can yield significantly different flux estimates depending on grid resolution. For the relatively homogeneous areas containing

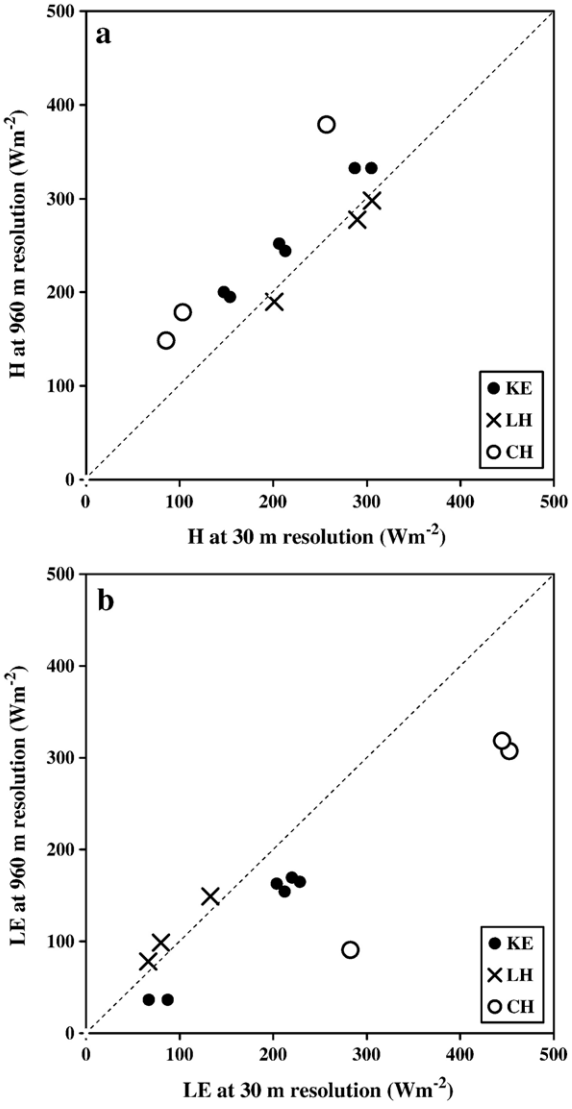

Fig. 9. Comparison TSM predictions of H and LE using high (30 m) and low (960 m) resolution thermal data for the three overpass days, integrated over the estimated tower source areas at Kendall (KE), Lucky Hills (LH) and Charleston (CH). Dashed line represents perfect agreement.

essentially a single land cover and no abrupt changes in fractional vegetation cover (e.g., Lucky Hills) the difference in model output between high and coarse resolutions is minor. For riparian sites such as Charleston, which show the largest intrinsic variability in surface temperature and vegetation cover conditions owing to marked changes in land cover class over distances ranging from 50 to 500 m, the differences at the two resolutions are as high as 200 W m^{-2} for LE. These findings are in agreement with results reported by Moran et al. (1997) who found significant discrepancies in the heat fluxes caused by aggregation errors (i.e., using fine versus coarse resolution remote sensing inputs) for this landscape.

5. Conclusions

Both in the validation of remote sensing-based land surface models with tower observations and in discriminating spatial patterns of latent heat flux due to land cover/land use and moisture/vegetation condition, a pixel resolution on the order of 10 m is highly desirable, although ~100 m pixel resolution still provides useful information on the spatial pattern and degree of contrast in range in moisture/vegetation conditions. At MODIS thermal resolution (~1000 m), much of the spatial variation in key TSM inputs (vegetation cover and surface temperature) is lost resulting in greater likelihood for large discrepancies with flux tower observations. This is due not only to the scale/resolution mismatch with source-area contributing eddy covariance sensor measurements (~100 m), but also errors in specification of the key model inputs for such mixed pixels, particularly when a pixel contains a riparian area adjacent to desert shrubland (Kustas & Norman, 2000a).

This study indicates that for landscapes containing significant fine scale (<1 km) variability in vegetation conditions (including cover amount, type and stress condition), the use of MODIS-resolution thermal data in a remote sensing-based model such as the TSM gives sub-optimal results.

Many landscapes have significant land use/land cover changes at the 10^2 m scale. This was the motivation for MODIS having a 250 m resolution visible/near-infrared band (Townshend & Justice, 1988). The thermal resolution of MODIS used with remote sensing-based energy balance model is too coarse for discriminating sharp contrasts in flux patterns caused by changes in land cover/land use or other environmental factors. A thermal sensor needs to have at least ~100 m resolution to facilitate model validation with respect to flux tower measurements and to detect significant changes in surface energy balance/flux partitioning between heat and water vapor. Currently, there are no plans to support such a high resolution thermal sensor on any future satellite platforms, including Landsat. Without such high resolution thermal data, remote sensing-based land surface models will have limited utility in assessing water use, vegetation stress, and other environmental metrics for agricultural and naturally heterogeneous landscapes.

Acknowledgements

We would like to thank Tom Jackson for his organization and coordination of the SMEX04 field project and the USDA-ARS Southwest Watershed Research Unit and Walnut Gulch Experimental Watershed personnel for their logistical support prior, during and after the SMEX04 field campaign.

References

Agam, N., Kustas, W. P., Anderson, M. C., Li, F., & Neale, C. M. U. (2007). A vegetation index technique for spatial sharpening of thermal imagery. *Remote Sensing of Environment*, *107*, 545–558.

Anderson, M. C., Norman, J. M., Kustas, W. P., Li, F., Prueger, J. H., & Mecikalski, J. R. (2005). Effects of vegetation clumping on two-source model estimates of surface energy fluxes from an agricultural landscape during SMACEX. *Journal of Hydrometeorology*, *6*, 892–909.

Anderson, M. C., Norman, J. M., Mecikalski, J. R., Torn, R. D., Kustas, W. P., & Basara, J. B. (2004). A multi-scale remote sensing model for disaggregating regional fluxes to micrometeorological scales. *Journal of Hydrometeorology*, *5*, 343–363.

Berk, A., Bernstein, L. S., Anderson, G. P., Acharya, P. K., Robertson, D. C., Chetwynd, J. H., et al. (1998). MODTRAN cloud and multiple scattering upgrades with application to AVIRIS. *Remote Sensing of Environment*, *65*, 367–375.

Choudhury, B. J. (1987). Relationships between vegetation indices, radiation absorption, and net photosynthesis evaluated by a sensitivity analysis. *Remote Sensing of Environment*, *22*, 209–233.

Choudhury, B. J., Ahmed, N. U., Idso, S. B., Reginato, R. J., & Daughtry, C. S. T. (1994). Relations between evaporation coefficients and vegetation indices studied by model simulation. *Remote Sensing of Environment*, *50*, 1–17.

Crow, W. T., Li, F., & Kustas, W. P. (2005). Intercomparison of spatially distributed models for predicting surface energy flux patterns during SMACEX. *Journal of Hydrometeorology*, *6*, 941–953.

Detto, M., Montaldo, N., Albertson, J. D., Mancini, M., & Katul, G. (2006). Soil moisture and vegetation controls on evapotranspiration in a heterogeneous Mediterranean ecosystem on Sardinia, Italy. *Water Resources Research*, *42*, W08419.

Diak, G. R., Mecikalski, J. R., Anderson, M. C., Norman, J. M., Kustas, W. P., Torn, R. D., et al. (2004). Estimating land-surface energy budgets from space: Review and current efforts at the University of Wisconsin—Madison and USDA-ARS. *Bulletin of the American Meteorological Society*, *85*, 65–78.

Eckman, R. M. (1994). Re-examination of empirically derived formulas for horizontal diffusion from surface sources. *Atmospheric Environment*, *28*, 265–272.

Emmerich, W. E. (2003). Carbon dioxide fluxes in a semiarid environment with high carbonate soils. *Agricultural and Forest Meteorology*, *116*, 91–102.

Foken, T., Wimmer, F., Mauder, M., Thomas, C., & Liebethal, C. (2006). Some aspects of the energy balance closure problem. *Atmospheric Chemistry Physics Discussions*, *6*, 3381–3402.

Goodrich, D. C., Chehbouni, A., Goff, B., MacNish, B., Maddock, T., Moran, S., et al. (2000). Preface paper to the Semi-Arid Land-Surface-Atmosphere (SALSA) program special issue. *Agricultural and Forest Meteorology*, *105*, 3–20.

Hsieh, C. I., Katul, G., & Chi, T. W. (2000). An approximate analytical model for footprint estimation of scalar fluxes in thermally stratified atmospheric flows. *Advances in Water Resources*, *23*, 765–772.

Humes, K. S., Kustas, W. P., Moran, M. S., Nichols, W. D., & Weltz, M. A. (1994). Variability of emissivity and surface temperature over a sparsely vegetated surface. *Water Resources Research*, *30*, 1299–1310.

Kim, J., Guo, Q., Baldocchi, D. D., Leclerc, M. Y., Xu, L., & Schmid, H. P. (2006). Upscaling fluxes from tower to landscape: Overlaying flux footprints on high-resolution (IKONOS) images of vegetation cover. *Agricultural Forest Meteorology*, *136*, 132–146.

Kustas, W. P., & Goodrich, D. C. (1994). Preface to special section on Monsoon '90. *Water Resource Research*, *30*, 1211–1225.

Kustas, W. P., & Norman, J. M. (1999). Evaluation of soil and vegetation heat flux predictions using a simple two-source model with radiometric temperatures for partial canopy cover. *Agricultural and Forest Meteorology*, *94*, 13–29.

Kustas, W. P., & Norman, J. M. (2000a). Evaluating the effects of sub-pixel heterogeneity on pixel average fluxes. *Remote Sensing of Environment*, *74*, 327−342.

Kustas, W. P., & Norman, J. M. (2000b). A two-source energy balance approach using directional radiometric temperature observations for sparse canopy covered surfaces. *Agronomy Journal*, *92*, 847−854.

Kustas, W. P., Norman, J. M., Anderson, M. C., & French, A. N. (2003). Estimating subpixel surface temperatures and energy fluxes from the vegetation index-radiometric temperature relationship. *Remote Sensing of Environment*, *85*, 429−440.

Kustas, W. P., Li, F., Jackson, T. J., Prueger, J. H., MacPherson, J. I., & Wolde, M. (2004a). Effects of remote sensing pixel resolution on modeled energy flux variability of croplands in Iowa. *Remote Sensing of Environment*, *92*, 535−547.

Kustas, W. P., Norman, J. M., Schmugge, T. J., & Anderson, M. C. (2004b). Mapping surface energy fluxes with radiometric temperature. Chapter 7. In D. Quattrochi & J. Luvall (Eds.), *Thermal remote sensing in land surface processes* (pp. 205−253). Florida, USA: CRC Press Boca Raton Book Chapter.

Li, F., Jackson, T. J., Kustas, W. P., Schmugge, T. J., French, A. N., Cosh, M., et al. (2004). Deriving land surface temperature from Landsat 5 and 7 during SMEX02/SMACEX. *Remote Sensing of Environment*, *92*, 521−534.

Li, F., Kustas, W. P., Prueger, J. H., Neale, C. M. U., & Jackson, T. J. (2005). Utility of remote sensing based two-source energy balance model under low and high vegetation cover conditions. *Journal of Hydrometeorology*, *6*, 878−891.

Moran, M. S., Humes, K. S., & Pinter, P. J., Jr. (1997). The scaling characteristics of remotely-sensed variables for sparsely-vegetated heterogeneous landscapes. *Journal of Hydrology*, *190*, 337−362.

Norman, J. M., Kustas, W. P., & Humes, K. S. (1995). A two-source approach for estimating soil and vegetation energy fluxes in observations of directional radiometric surface temperature. *Agricultural and Forest Meteorology*, *77*, 263−293.

Santanello, J. A., & Friedl, M. A. (2003). Diurnal covariation in soil heat flux and net radiation. *Journal of Applied Meteorology*, *42*, 851−862.

Scott, R. L., Edwards, E. A., Shuttleworth, W. J., Huxman, T. E., Watts, C., & Goodrich, D. C. (2004). Interannual and seasonal variation in fluxes of water and carbon dioxide from a riparian woodland ecosystem. *Agricultural Forest Meteorology*, *122*, 65−84.

Stannard, D. I., Blanford, J. H., Kustas, W. P., Nichols, W. D., Amer, S. A., Schmugge, T. J., et al. (1994). Interpretation of surface-flux measurements in heterogeneous terrain during the Monsoon '90 experiment. *Water Resource Research*, *30*, 1227−1239.

Stewart, J. B., Kustas, W. P., Humes, K. S., Nichols, W. D., Moran, M. S., & de Bruin, H. A. R. (1994). Sensible heat flux-radiometric surface temperature relationship for 8 semi-arid areas. *Journal of Applied Meteorology*, *33*, 1110−1117.

Townshend, J. G. R., & Justice, C. O. (1988). Selecting the spatial resolution of satellite sensors required for global monitoring of land transformations. *International Journal of Remote Sensing*, *9*, 187−236.

Twine, T. E., Kustas, W. P., Norman, J. M., Cook, D. R., Houser, P. R., Meyers, T. P., et al. (2000). Correcting eddy-covariance flux underestimates over a grassland. *Agricultural and Forest Meteorology*, *103*, 279−300.

Verhoef, A., De Bruin, H. A. R., & van den Hurk, B. J. J. M. (1997). Some practical notes on the parameter kB^{-1} for sparse vegetation. *Journal of Applied Meteorology*, *36*, 560−572.

Wilson, K., Goldstein, A., Falge, E., Aubinet, M., Baldocchi, D., Berbigier, P., et al. (2002). Energy balance closure at FLUXNET sites. *Agricultural and Forest Meteorology*, *113*, 223−234.

Zhan, X., Kustas, W. P., & Humes, K. S. (1996). An intercomparison study on models of sensible heat flux over partial canopy surfaces with remotely sensed surface temperature. *Remote Sensing of Environment*, *58*, 242−256.